Title

Pharmacokinetics of rifapentine and rifampin in a rabbit model of tuberculosis and correlation with clinical trial data

Journal

Science Translational Medicine, 10(435)

ISSN

1946-6234

Authors

Rifat, Dalin
Prideaux, Brendan
Savic, Radojka M
et al.

Publication Date

2018-04-04

DOI

10.1126/scitranslmed.aai7786

Peer reviewed

HHS Public Access

Author manuscript

Sci Transl Med. Author manuscript; available in PMC 2019 April 04.

Published in final edited form as:

Sci Transl Med. 2018 April 04; 10(435): . doi:10.1126/scitranslmed.aai7786.

Pharmacokinetics of rifapentine and rifampin in a rabbit model of tuberculosis and correlation with clinical trial data

Dalin Rifat[1], **Brendan Prideaux**[2], **Radojka M. Savic**[3], **Michael E. Urbanowski**[1], **Teresa L. Parsons**[1], **Brian Luna**[4], **Mark A. Marzinke**[1], **Alvaro A. Ordonez**[1], **Vincent P. DeMarco**[1], **Sanjay K. Jain**[1], **Veronique Dartois**[2], **William R. Bishai**[1], and **Kelly E. Dooley**[1,*]

[1]Johns Hopkins University School of Medicine, Baltimore, MD 21205, USA

[2]Rutgers New Jersey Medical School, Public Health Research Institute, Newark, NJ 07103, USA

[3]Department of Bioengineering, University of California at San Francisco School of Pharmacy, San Francisco, CA 94117, USA

[4]Department of Medicine, University of Southern California Keck School of Medicine, Los Angeles, CA 90033, USA

Abstract

In clinical trials of two rifamycin antibiotics (rifampin and rifapentine) for treating tuberculosis (TB), patients with cavitary lung lesions did not appear to derive benefit from rifapentine. Rifapentine was found not to outperform rifampin, despite a lower minimum inhibitory concentration against *Mycobacterium tuberculosis* in mouse models of TB. To understand these findings, we have developed a rabbit model of TB that reliably develops lung cavities with features similar to those of patients with pulmonary cavitary TB. After single or multiple doses of rifampin

*Corresponding author: kdooley1@jhmi.edu.

SUPPLEMENTARY MATERIALS

www.sciencetranslationalmedicine.org/cgi/content/full/10/435/eaai7786/DC1

Materials and Methods

Fig. S1. Concentration-time curve in plasma and lung tissue after a single dose of 30 mg/kg rifapentine administered to healthy rabbits.

Fig. S2. Concentration-time curve for rifampin and rifapentine in plasma and lung lesions after a single drug dose in rabbits with pulmonary cavitary TB.

Fig. S3. Concentration-time curve for rifampin or rifapentine in plasma after multiple doses in rabbits with cavitary TB sacrificed 2 or 12 hours after the final drug dose.

Fig. S4. Absolute drug concentrations of rifampin or rifapentine in different compartments of lung lesions after single or multiple doses in rabbits with pulmonary cavitary TB.

Fig. S5. PK model describing tissue penetration of rifampin and rifapentine.

Table S1. PK parameters of rifampin and rifapentine in plasma and in lung lesions after a single drug dose.

Author contributions: D.R., B.P., R.M.S., B.L., M.A.M., S.K.J., V.D., W.R.B., and K.E.D. conceived the study and designed the experiments. Rabbit pulmonary cavitary TB models and dosing experiments were conducted and analyzed by D.R., M.E.U., and W.R.B. LC-MS/MS was performed by T.L.P. and M.A.M. and all the data were analyzed by D.R. MALDI-MSI was performed and analyzed by B.P. and V.D. PET-CT was carried out and analyzed by A.A.O., V.P.D., and S.K.J. Mathematical (PK/PD) modeling was performed by R.M.S. D.R. and K.E.D. drafted the manuscript and R.S., B.P., M.E.U., T.L.P., M.A.M., and A.A.O. contributed to writing the paper. D.R., B.P., R.M.S., M.E.U., M.A.M., S.K.J., V.D., W.R.B., and K.E.D. edited the manuscript.

Competing interests: R.M.S. is a consultant to Amgen, Global Blood Therapeutics, and MedImmune and is the owner/co-founder of Insight Rx Inc. All other authors declare that they have no competing interests.

Data and materials availability: All data needed to evaluate the conclusions in the paper are present in the paper and/or the Supplementary Materials. Additional data related to this paper may be requested from the authors. The antibiotic drugs rifampin and rifapentine were provided by Sanofi under a material transfer agreement.

or rifapentine that produced human-equivalent plasma exposures, rabbits were sacrificed at different time points after dosing. We measured site-of-disease drug pharmacokinetics and tissue drug distribution. We used pharmacokinetic-pharmacodynamic (PK/PD) modeling to estimate drug penetration into different types of tubercular lesions. Both drugs penetrated rabbit lung cellular lesions, as well as the fibrotic cavity wall of cavitary lesions (penetration coefficients ≥1 compared to plasma). For the necrotic liquefied material inside cavitary lesions known as caseum (which contains high numbers of bacteria), the penetration coefficient was 1.0 for rifampin but only 0.25 for rifapentine. When estimates of site-of-disease drug PK were substituted into clinical PK/PD models, the relationship between site-of-action exposure and sputum culture conversion was significant ($P < 10^{-7}$). We propose that poor penetration of rifapentine into lung cavitary lesions explains, in part, why rifapentine doses required to improve treatment outcomes in two phase 2 clinical trials were four times higher in TB patients with large cavities compared to TB patients without cavitary lung disease.

INTRODUCTION

Mycobacterium tuberculosis (Mtb) is the bacterial pathogen that causes tuberculosis (TB). In 2016, there were 10.4 million incident TB cases and 1.67 million TB-related deaths. TB has now surpassed HIV as the number one infectious disease worldwide (1). Despite the availability of effective anti-TB drugs, the current TB four-drug regimen takes at least 6 months to treat drug-sensitive Mtb. A drug regimen that can clear Mtb more rapidly is urgently needed for global TB control efforts. Understanding the pharmacokinetics (PK) of anti-TB drugs at the sites of infection, where the Mtb bacilli reside and where drugs must exert their bactericidal activity, is necessary for optimizing drug regimens for different forms of TB disease and for shortening TB treatment duration (2).

In the standard 6-month TB treatment regimen, rifampin, an inhibitor of DNA-dependent RNA polymerase, plays a key role in clearing bacterial infection. It is particularly effective at killing semidormant or dormant bacilli (3). Rifapentine is a cyclopentyl ring–substituted rifamycin with a longer half-life and lower minimum inhibitory concentration against Mtb than rifampin. Rifapentine has been actively investigated as a potential substitute for rifampin that could be the basis for a shortened TB treatment regimen (4–6). Studies in well-established murine models of TB disease showed that regimens containing daily rifapentine at doses producing similar plasma exposures to those achieved with a 10-mg/kg dose in humans, led to clearance of Mtb in mice in 3 months when used instead of rifampin and combined with standard companion drugs (isoniazid, pyrazinamide, and ethambutol) (7). However, in a phase 2 clinical trial, substitution of standard-dose (10 mg/kg) rifampin with an empiric dose of 10 mg/kg of rifapentine (producing plasma exposures akin to those seen in the mouse models) was not more efficacious. Specifically, microbiological outcomes were similar for both antibiotics: Sputum culture conversion rates to negative on solid and liquid media after 8 weeks of treatment were 83.3 and 65.1% for rifampin and 86.4 and 67.9% for rifapentine, respectively (5). In a subsequent dose-escalation phase 2 clinical trial, using high-dose daily rifapentine (15 or 20 mg/kg), instead of rifampin (in combination with the standard first-line drugs isoniazid, pyrazinamide, and ethambutol), improved the antimicrobial activity of combination chemotherapy for pulmonary TB (4). Higher drug

exposures were associated with quicker time to culture conversion overall. However, those TB patients with large cavitary lung lesions who received rifapentine had similar rates of culture conversion as did those patients assigned to the rifampin arm (even when drug exposures were relatively high), suggesting that there was a TB patient population who had not benefitted from rifapentine, even at high doses, at least in the first 2 months of therapy (8).

The pathology of pulmonary TB disease in human patients is characterized by the development of heterogeneous lesions; the most common types include cellular granulomas (cellular lesions), small granulomas containing a caseous necrotic center (necrotic lesions), and larger lesions that develop into cavities with liquefied contents full of Mtb bacilli and are surrounded by a thick fibrotic wall (cavitary lesions) (9, 10). Mouse models of TB have intracellular disease in which Mtb resides within lung macrophages, and they do not develop large cavitary lung lesions (7). Studies using matrix-assisted laser desorption/ionization mass spectrometry imaging (MALDI-MSI) and liquid chromatography–tandem mass spectrometry (LC-MS/MS) have shown that drugs against TB exhibit different trends in the rate and extent of penetration into lung lesions in mouse and rabbit models (2, 11). It remains unknown whether rifapentine has limited penetration into the large cavitary lesions that characterize human disease, which are not present in existing mouse and rabbit models. It is also not clear whether rifapentine and rifampin differ in their penetration into these lesions, given that rifapentine displays somewhat higher protein binding (97 to 99%) than does rifampin (80 to 85%) (12).

The rabbit cavitary pulmonary model of TB that we have developed has necrotic granulomas and cavitary lesions similar to human TB pathology, which makes it a potentially useful tool for evaluating penetration of rifampin and rifapentine into these types of lesions (13). Here, we optimized our rabbit cavitary TB model to produce heterogeneous lesions in the animals after aerosol infection with Mtb and large cavitary lesions after bronchoscopic infection with Mtb. The goal of the current study was to use this rabbit model to evaluate the PK of rifampin and rifapentine over time at sites of Mtb infection using multiple modalities and to link these results to findings in phase 2 clinical trials.

RESULTS

Drug solubility and half-life of rifampin and rifapentine in rabbits

Rifampin dissolved readily in a vehicle solution at 5 mg/ml and was stable for up to 5 days at 4°C and for 24 hours at room temperature. Rifapentine did not dissolve readily, and it precipitated out of solution at pH values <10. Adjustment with 10 M sodium hydroxide to pH 10.5 and stirring overnight at 4°C (or sonication for 2.5 hours at room temperature, followed by stirring at room temperature for at least 6 hours) was required to dissolve the drug completely in a solution (10 mg/ml). Given the high pH of the solution, rapid bolus dosing was poorly tolerated by the rabbits. A slower infusion over 10 to 15 min was well tolerated with no signs of distress.

The PK of rifapentine has not been studied previously in rabbits. With a dose of 30 mg/kg, rifapentine peak concentration (C_{max}) in plasma measured 30 min after intravenous infusion

was 33 μg/ml, with a log-linear decline to 0.87 μg/ml at 15 hours after dosing. The area under the concentration-time curve ($AUC_{0–15}$) was 170 μg·hour/ml, and the half-life ($T_{½}$) was 4 hours (fig. S1). By way of comparison, doses of rifapentine of 10, 15, and 20 mg/kg in adult patients with TB achieve median C_{max} values of 15, 21, and 28 μg/ml and median $AUC_{0–24}$ of 279, 387, and 537 μg·hour/ml, respectively; rifapentine has a $T_{½}$ in human patients of about 16 hours (4). The concentration of rifapentine in healthy rabbit lung tissue following a single dose of 30 mg/kg administered intravenously was 13 μg/g 2 hours after dosing; the $AUC_{0–15}$ was 82 μg·hour/ml with a tissue $T_{½}$ of 6.7 hours; rifapentine was undetectable 15 hours after dosing (fig. S1). After a single 10-mg/kg dose of rifampin administered intravenously, plasma C_{max} was 17 μg/ml and $AUC_{0–6}$ was 45 μg·hour/ml [compared with 7.5 μg/ml and 45 μg·hour/ml, respectively, in human patients following a 10-mg/kg oral dose (6)] (fig. S2A). On the basis of PK modeling of these data, doses of 10 mg/kg once daily of rifampin and 60 mg/kg once daily of rifapentine divided into several smaller doses administered every 3 or 4 hours were predicted to achieve similar daily AUCs as clinical doses of rifampin (10 mg/kg) and rifapentine (10 mg/kg), as well as quantifiable concentrations in rabbit lung tissue (fig. S2B).

Optimizing a rabbit model of pulmonary cavitary TB

We used two methods to produce tubercular lesions in rabbits. First, to generate the spectrum of lesions found in human TB (granulomas, fibrotic granulomas, caseous lesions, and cavities), we subjected rabbits to aerosol infection. Rabbits infected via the aerosol route developed multiple dense areas of consolidation (inflammatory lesions due to Mtb infection) by 7 weeks as shown by computed tomography (CT) analysis. Fifty percent of the rabbits developed lung cavities by 9 weeks after infection; cavities were 0.3 to 1.0 cm in diameter. These aerosol-infected rabbits were used in single-dosing experiments.

To model lung destruction, such as that observed in TB patients who have extensive cavitary disease, we developed a bronchoscopic delivery system in which a high-burden Mtb inoculation was targeted to a specific rabbit lung lobe. The goal was to produce stable, nonfatal cavitary TB more reliably and quickly than is typically achieved with aerosol infection and to elicit lesions in specific lobes of the lung. In “infectious dose ranging” experiments, we deposited Mtb at densities ranging from 5×10^4 to 5×10^8 colony-forming units (CFU)/ml at volumes of Mtb suspension ranging from 0.15 to 1.2 ml by bronchoscope and examined disease progression by CT imaging (Table 1). Small volume delivery of a high bacterial density suspension to the rabbits reliably produced cavities within 4 weeks. Lower doses produced no disease, and higher doses produced severe, life-threatening disease.

Gross examination and histopathology of diseased lung tissue from both aerosol- and bronchoscope-infected rabbits (Fig. 1A) confirmed human-like TB pathology, with diverse lesions, including cellular lesions, small necrotic lesions, and cavitary lesions comprising necrotic caseum in the center surrounded by a thick fibrotic wall (Fig. 1, B to D). The diameter of cavities varied from 0.3 to 1.5 cm. Hematoxylin and eosin (H&E) staining confirmed human-like TB histopathology, including cavitary lesions filled with necrotic debris (Fig. 1, D to F). Serial acid-fast preparations showed that regions of high bacterial density were confined to caseous regions of cavities (Fig. 1G). Within caseous regions, the

density of bacteria varied (Fig. 1, G2 and G3). Bacilli were rarely observed in non-necrotic regions of the lung cavity walls (Fig. 1, G1 and G4). The high density of Mtb bacteria in caseum and scarcity in non-necrotic granulomas is a pathological feature observed in human TB.

Penetration of rifampin and rifapentine into TB pulmonary lesions in rabbits

Measurement of plasma and tissue PK by LC-MS/MS demonstrated that after a single dose, both rifampin and rifapentine penetrated well into uninvolved lung tissue, cellular lesions, and tissues surrounding cavitary lesions, as early as 2 hours after dosing (Fig. 2, fig. S4, and table S1). Clearance of rifampin from lung tissue appeared to be slower than clearance from plasma, as a longer $T_{½}$ was observed in lung tissue than in plasma (fig. S2 and table S1). Clearance of rifapentine from tissue lesions was similar to clearance from plasma with similar $T_{½}$ and AUC $_{0–6}$ (fig. S2 and table S1).

Concentrations of both rifampin and rifapentine were lower in the center of necrotic lesions and cavity caseum than in healthy lung tissue or cellular lesions, particularly in the first hours after dosing. The concentration of rifampin in the cavity caseum was half that of cellular lesions 2 hours after dosing. The concentration of rifapentine in cavity caseum was 4 to 4.2 and 5.4 to 5.7 times less than that in cellular lesions and cavity walls 3 and 6 hours after a single dose, respectively ($P < 0.001$) (fig. S4). Figure 2(A to C) shows the tissue-to-plasma drug concentration ratio after a single dose of rifampin or rifapentine.

The plasma PK of rifampin following multiple doses is shown in fig. S3. AUC $_{0–26}$ was estimated to be 525 μg·hour/ml. After multiple doses, the 2-hour post-dose concentration of rifampin was higher than that of a single dose for all lesion types ($P < 0.01$) (fig. S4). By 12 hours after dosing, rifampin concentrations in all lesion types were reduced compared to the 2-hour post-dose concentrations ($P < 0.02$), except for the cavity caseum where 12-hour post-dose concentrations were significantly higher than 2-hour post-dose concentrations ($P < 0.05$) (fig. S4). For rifapentine, the plasma PK after multiple doses with an $AUC_{0–23}$ was estimated to be 1813 μg·hour/ml (fig. S3). For rifapentine, after multiple doses, the 2-hour post-dose concentrations were not significantly higher than the 2- to 3-hour post-dose concentrations after a single dose (fig. S4). Between 2 and 12 hours after dosing, rifapentine in the cavity caseum increased ($P > 0.05$), whereas rifapentine in other lung tissue lesions decreased ($P < 0.02$) (fig. S4). The cellular lesion–to-plasma ratio, cavity wall–to-plasma ratio, and cavity caseum–to-plasma ratio, 2 hours after the last of multiple doses of rifampin or rifapentine, were twofold, 2.2-fold, and 6.4-fold higher for rifampin compared to rifapentine ($P = 0.0002$, 0.0001, and 0.03, respectively) (Fig. 2D). Similarly, for rifampin, the tissue-to-plasma ratios were higher than the rifapentine tissue-to-plasma ratios at 12 hours after dosing. Notably, the cavity caseum-to-plasma ratio for rifampin was 22-fold higher than that for rifapentine ($P < 0.0005$ to 0.03) (Fig. 2E).

Linking drug PK in the rabbit cavitary TB model to clinical trial data

All plasma, tissue, and intralesional PK values from single- and multiple- dosing experiments with rifampin and rifapentine were incorporated into PK models (fig. S5). For rifampin, the penetration coefficient (ratio of drug in tissue compared to plasma) for all

lesion types—cellular lesions, tissue surrounding lesions, cavity caseum, and cavity wall—was close to 1.0 (Table 2). For rifapentine, the penetration coefficients for cellular lesions, tissue surrounding lesions, and cavity wall were also close to 1.0, whereas for cavity caseum, the penetration coefficient was 0.25 (Table 2). In uninvolved lung tissue for both rifampin and rifapentine, the tissue-to-plasma ratios were ~0.7 to 0.8.

Using previously developed PK-pharmacodynamic (PK/PD) exposure-response models for clinical trials with TB patients who had received rifapentine at doses of 10 to 20 mg/kg (4, 8), we substituted site-of-disease PK for the TB patient plasma PK in these models (assuming that site-of-action drug concentrations were 25% of plasma concentrations for patients with large lung cavities). This improved the likelihood that the model would fit the data as evidenced by the substantial decrease in objective function values (−2 log likelihood), resulting in a highly significant relationship between site-of-action exposure and sputum culture conversion ($P < 10^{-7}$). The estimated site-of-action AUC_{50} was 207 μg·hour/ml.

Spatial distribution of rifampin and rifapentine shown by MALDI-MSI and PET-CT imaging

The results of MALDI-MSI were consistent with our findings by LC-MS/MS (Figs. 3 and 4). A lower drug concentration was observed in cavity caseum compared to cellular lesions after a single dose of rifampin or rifapentine (Fig. 3). At the 2-hour post-dose time point after multiple dosing, rifampin was highly localized to the cellular area of the cavitary lesions with limited penetration into the caseum (Fig. 4A). By the 12-hour post-dose time point, rifampin had successfully penetrated the entire lesion and was more highly concentrated in the cavity caseum than the surrounding cavity wall (Fig. 4A). Rifapentine tissue distribution was similar after single or multiple doses, with the highest drug concentration observed in the cavity wall and cellular lesion areas (Figs. 3 and 4B). H&E staining was used to verify histopathology of lesion biopsies and confirmed our gross examination (Figs. 3 and 4).

To investigate whether noninvasive positron emission tomography (PET)–CT imaging provided similar drug distribution data to MALDI-MSI and LC-MS/MS, we used PET-CT with ^{11}C-labeled rifampin to image cavitary lesions in Mtb-infected rabbits (Fig. 5A). Dynamic PET-CT imaging was performed for 55 min after intravenous injection of ^{11}C-rifampin as a microdose (Fig. 5B). ^{11}C-rifampin distributed rapidly and widely (Fig. 5, C and D), and the ^{11}C-rifampin PET signal was evenly distributed in uninvolved lung tissues and in infected lung parenchyma. Lower concentrations of rifampin were noted in cavitary lesions compared to the infected lung parenchyma ($P < 0.001$) (Fig. 5E).

DISCUSSION

Shortening the duration of TB drug treatment may help global efforts to control TB, but an effective regimen of 4 or fewer months' duration has been stubbornly elusive, as has a predictive translational animal model. Optimization of rifamycin antibiotics remains among the most promising treatment-shortening strategies given their unique activity against "persister" Mtb bacilli that must be eradicated to effect cure (14). Replacing rifampin with rifapentine has been of great interest, given rifapentine's lower minimum inhibitory

concentration against Mtb compared to rifampin and also because of the promising activity in mouse models of TB. For example, replacing rifampin with rifapentine was highly effective in the well-established BALB/c mouse model of pulmonary TB (7). However, treating TB patients with rifapentine instead of rifampin (at doses that produced similar plasma concentrations as those used in the successful mouse studies) did not improve sputum conversion rates in a phase 2 clinical trial (5). Given that TB in human patients is characterized by diverse types of pathology, including large cavitary lesions that are absent from standard mouse models, and the fact that rifapentine is highly protein-bound, we hypothesized that rifapentine may have limited penetration into cavity caseum lesions relative to rifampin. Here, we developed a rabbit model with human-like TB pathology, specifically lung cavities with caseous necrotic contents and a fibrotic rim with a surrounding cellular infiltrate. We then measured drug concentrations in multiple disease lesions in this rabbit model after delivery of rifampin or rifapentine at doses intended to achieve clinically relevant plasma concentrations. Through PK modeling, we discovered that rifapentine penetration into cavity caseum was 75% less than that in other lesion types, which may explain the poor performance of rifapentine in TB patients with large lung cavitary lesions in two phase 2 clinical trials, even given the higher rifapentine doses used (8).

Several tools are currently used for developing TB drug regimens, including in vitro cellular systems and animal models, most notably mouse models (15). The mouse model recapitulates many aspects of drug effects in TB patients, allowing us to select those drug combinations that are most promising for treatment of clinical TB. The well-validated BALB/c mouse model develops small cellular granulomas and is characterized by disease largely confined to macrophages (7). The C3HeB/FeJ or Kramnik mouse model that develops small necrotic granulomas and occasionally small cavities (16) and nude mice provide valuable information about the effects of diverse pathology and immunodeficiency, respectively, on drug efficacy and the emergence of drug resistance (17, 18). However, with available models, we are still unable to predict drugs and doses that will result in shortening of the treatment duration for TB patients. This knowledge gap and lack of a fully translational animal model has contributed to costly phase 3 clinical trial failures (19–21).

Cavitary lung disease is a known risk factor for relapse in TB patients after drug treatment, presumably because bacterial burden is higher in the cavity lesions. To exert their antibacterial effects, anti-TB drugs must penetrate into large necrotic lesions and diffuse across the caseum that is rich in proteins and lipids (22, 23). A reliable animal model that develops large lung cavities with necrotic, bacilli-filled caseum akin to the human disease would help to fill gaps in our understanding of drug distribution in lung tissue and penetration into disease lesions where the “hard-to-reach” Mtb bacteria reside. Experimental models of rabbit cavitary TB have been developed previously (24, 25). Aerosol infection of rabbits with Mtb produces multiple lesion types, including cavities, akin to those in the human disease, but the success rate is variable and the time from experiment initiation to development of cavities is unpredictable (26). In a series of “infectious dose finding” experiments, we expanded our previous work and the work of others to infect rabbits with Mtb by bronchoscopic instillation, which produces large cavities in the lung lobe of interest within 4 weeks (24, 25) without causing severe infection. This model is less likely to

produce the complex, multifocal disease that aerosol infection produces. We hope that optimization of the rabbit model of lung cavitary TB may provide useful information for assessing drug distribution in lung cavitary lesions.

A new preclinical model is only useful if it can help to inform clinical trial design or predict outcomes. Previous PK/PD modeling of clinical data suggested that there was a strong correlation between plasma drug concentration and microbiological outcomes, such as sputum conversion, but those models did a poor job of explaining drug exposure-response relationships for the hardest-to-treat TB patients (8). When we substituted site-of-action PK for rifapentine into the PK/PD models (assuming tissue lesion to plasma ratios of 0.25 for patients with large lung cavities and 1.0 for all other patients based on the rabbit drug penetration data), the model fit improved substantially. To achieve an AUC_{50} of 207 μg·hour/ml, the average TB patient would require a minimum dose of 1800 mg (producing a plasma $AUC_{0–24}$ of 828 μg·hour/ml) to achieve that concentration of rifapentine in the cavity caseum, a dose that may fall outside the limits of tolerability (8, 27). TB patients with, for example, HIV co-infection, may need to be treated with higher doses of rifapentine.

For rifampin, cavitary disease was not as strong a predictor of microbiological outcomes in PK/PD analyses of clinical trial data (8), despite the higher pretreatment bacterial load in TB patients with cavities, potentially because rifampin penetrates well into all lesion types. In a recent study in patients with resistant TB scheduled to undergo lung resection who received multiple doses of rifampin pre-operatively, rifampin concentrations were as high or higher in cavity caseum than in healthy lung tissue or plasma, demonstrating that rifampin penetration into cavitary lesions in both the rabbit lung cavitary model and human cavitary TB was similar (2). Rifampin is 80 to 85% protein-bound, whereas rifapentine is 97 to 99% protein-bound (22), which may, in part, account for differences in intralesional distribution between these two otherwise structurally similar rifamycin antibiotics. Penetration of anti-TB drugs into tubercular lesions is known to vary greatly across drugs and may depend on factors, such as the drug’s size, lipophilicity, solubility, binding to plasma proteins, and transport into Mtb bacteria (22). The penetration of drugs into necrotic material or caseum appears to be dependent only on the free drug fraction because the drugs are distributed through passive diffusion due to lack of a vascular supply and are not actively transported (22). Sarathy *et al.* (22) used a rapid equilibrium dialysis assay to show that the fraction of unbound rifampin is 10 times higher than that of rifapentine in rabbit caseum ex vivo. They also showed that binding to caseum macromolecules is inversely proportional to passive diffusion into the necrotic core of caseous lesions and cavities (22), which is consistent with our finding that rifampin diffuses more effectively than rifapentine into caseum. It is unclear to what extent information about diffusion through caseum should be incorporated into decision-making during early development of potential anti-TB drugs, because the location and quantity of Mtb bacilli during treatment is unknown. However, it is clear that in combination therapy, drugs must be present in their free or unbound form at sufficient concentrations in lung lesions to protect against the emergence of drug-resistant bacteria. Thus, site-of-action PK for different drugs in a proposed regimen can inform dose selection to safeguard against intralesional “monotherapy”. Knowledge of PK in cavity caseum may be especially valuable given the high bacterial load in these lesions and the fact that these lesions are “pharmacological sanctuaries” given their diffusion-limiting content.

Mimicking human tissue drug PK in animal models is never straightforward. Here, rifampin and rifapentine were administered intravenously to avoid the variability in absorption that occurs when animals are dosed via oral gavage (11). Using model-based analyses of PK data from healthy rabbits, doses and frequencies of intravenous infusions were determined, which produced plasma AUC and C_{max} in clinically relevant ranges for the Mtb-infected rabbit experiments (despite the differences in rifapentine half-life between humans and rabbits). Thus, every effort was made to produce human-like disease pathology and clinically relevant drug concentrations, so that results from drug distribution experiments would be as informative as possible.

In our study, MALDI-MSI provided detailed semiquantitative spatial information regarding drug distribution that supplemented the LC-MS/MS data by enabling visualization of drugs and metabolites within distinct cellular locations in rabbit lung lesions where Mtb bacteria are known to reside. PET-CT imaging was also used as a proof-of-concept noninvasive component of this study to demonstrate drug concentrations in cavity caseum over time after dosing, without the need for necropsy. A PET-CT radioactive tracer validated in animal models could subsequently be used in TB patients to assess distribution of anti-TB drugs in multiple tissue compartments, including disease sites that are not readily accessible, such as those in the lung, bone, and brain.

Our study has several limitations. Free drug concentrations cannot be measured readily in the tissue, so we reported total drug concentrations. Also, given that necropsy was required to measure tissue PK, we did not obtain PK data for all time points after dosing. With the PK tissue distribution model that incorporates all data points, however, we could provide a mathematical description of drug distribution in rabbit plasma, lung tissue, and disease lesions that represented a tissue distribution model. This model should enable further simulations of rifampin and rifapentine PK at different lesion sites after different dosing regimens. Last, note that this is a drug distribution model, not a treatment model. There are no phase 3 clinical trial results to show whether the predictions of this model are correct. However, a phase 3 clinical trial of high-dose rifapentine is currently enrolling TB patients worldwide(clinicaltrials.govno.NCT02410772); results will be used to enhance the current model and further define its potential role in drug development.

In conclusion, we developed a rapid, predictable rabbit lung cavitary TB animal model. Using this rabbit model, we mathematically modeled site-of-disease PK and PK/PD for rifampin and rifapentine antibiotics. We determined that rifampin and rifapentine differed in their penetration into cavity caseum, a protein/lipid-rich, poorly vascularized area of cavitary lesions that is high in Mtb bacterial load. We incorporated these findings into existing PK/PD models from phase 2 clinical trials and found that site-of-action PK improved model fit and may help to explain why TB patients with large cavities did not appear to benefit from rifapentine at doses that were highly effective in TB patients with small or no cavities. Our model may serve as a tool to help optimize TB drug regimens by predicting drug distribution in disease lesions where Mtb resides and where anti-TB drugs must exert their bactericidal effects.

MATERIALS AND METHODS

Study design

This study was designed to provide mechanistic insight into differences in drug treatment response (time to stable culture conversion of sputum samples) reported in two phase 2 clinical trials of TB patients treated with rifampin or rifapentine. TB patients with large lung cavities (≥4 cm) treated with rifapentine took significantly longer to achieve culture conversion than did TB patients with smaller or no lung cavities treated with rifapentine, despite high plasma concentrations of the drug. This was not found in TB patients treated with rifampin. To help explain the differences in treatment responses between the two drugs (and elucidate a mechanistic reason for these differences), we designed experiments in a rabbit model of lung cavitary TB to quantify the tissue-to-plasma penetration ratio of rifampin and rifapentine in the different types of lung lesions that characterize pulmonary TB. To facilitate optimal experimental design, we initially performed PK experiments in healthy rabbits to characterize rifampin and rifapentine PK and to ensure that the sampling scheme for collection of rabbit tissue and plasma samples for PK analysis was optimal. We also elected to administer drug intravenously to minimize the “noise” in plasma PK that can arise from variable absorption and to maximize the signal from measurements of the tissue to plasma penetration ratio (11). We measured drug concentrations in plasma and diseased lung tissue from rabbits infected with Mtb and calculated the tissue-to-plasma ratio for single and multiple doses of rifampin and rifapentine. Then, we applied these data to the phase 2 clinical trial data and performed new PK/PD analyses. In these analyses, we replaced plasma drug concentration with site-of-action drug concentration, assuming that TB patients with large cavities would also exhibit the same penetration ratio as estimated in the preclinical animal model.

Rabbit pulmonary cavitary TB model

New Zealand White female rabbits (2.8 to 3.6 kg of body weight) were purchased from Robinson Services Inc. All procedures followed the approval of the Johns Hopkins University Institutional Animal Care and Use Committee. *Mtb* H37Rv strain from frozen stock was grown to mid-log phase (optical density; OD_{600nm} = 0.5) and diluted in phosphate-buffered saline for use. Rabbits were housed in individual cages in a biosafety level 3 (BSL-3) animal facility.

Aerosol infection—Using a Madison Chamber Aerosol Infection Device (University of Wisconsin), *Mtb* H37Rv in a suspension of 10^5 CFU/ml was used to infect rabbits. A group of 12 rabbits was subjected to five low-dose infections over the course of two and a half weeks. By 5 weeks after the final exposure, the rabbits underwent CT scans weekly to evaluate progress of the disease and formation of cavities.

Bronchoscopic infection—For bronchoscopic infection, 18 rabbits were presensitized with heat-killed *Mycobacterium bovis* in a BSL-2 animal facility (28); the animals were subsequently transferred to a BSL-3 facility and were then challenged with *Mtb* H37Rv (24). More specifically, rabbits were administered a series of five subcutaneous injections of a 1:1 suspension of Freund’s incomplete adjuvant mixed with 1×10^8 heat-killed bacilli. The

injections were spread out over two and a half weeks, and the rabbits were subsequently allowed to rest for another two and a half weeks, followed by a purified protein derivative testing to confirm sensitization. The rabbits were anesthetized as previously described and then positioned on a table followed by bronchoscopic infection with *Mtb* H37Rv (Olympus, WM-NP2 EXERA III Mobile Endoscopic Workstation) through 4.0-mm outer diameter endotracheal tube and 35.5 inches of 1.5-mm outer diameter catheter tubing (0.3 ml of dead space) (Fig. 1A). The rabbits were divided into several groups. *Mtb* H37Rv was deposited in the upper and lower lobes of the left and right lungs (two to three locations per lung) in different groups of rabbits, at variable infectious doses (5×10^4 to 5×10^8 CFU/ml, volume per instillation of 0.15 to 1.2 ml) (Table 1). After 2 weeks of exposure, animals underwent weekly chest CT scans to assess the extent of disease and cavity formation in the lung. The CFU of the infecting suspension (for both aerosol infection and bronchoscope instillation) was determined by serial dilution and plating on 7H11 agar plates.

Dosing experiments in healthy rabbits

Initially, uninfected rabbits were administered with rifampin or rifapentine, so that we could observe the tolerability of rifampin and rifapentine solutions and optimize the conditions for MALDI-MSI and LC-MS/MS for subsequent dosing experiments in infected animals. Drug solutions were formulated to achieve doses of 10 mg/kg of rifampin and 30 mg/kg of rifapentine for rabbits of 4 kg of body weight, so 8 ml of 5 mg/ml of rifampin and 12 ml of 10 mg/ml of rifapentine were prepared before intravenous administration to healthy rabbits, as described above. The tolerability of drug solutions was closely observed, and blood was sampled at 30 min after dosing and at the time of sacrifice for measurement of drug concentrations in plasma. For drug concentrations in lung tissues, rabbits were sacrificed 1 hour after dosing following anesthetization and euthanasia with 3 ml of euthasol euthanasia solution via the catheterized marginal vein. During the necropsy, the lungs were harvested, and the lung tissues were collected from upper, middle, and lower lobes in left and right lungs to evaluate the correlation between drug yield and the amount of processed lung tissue, as well as between drug yield and the location where lung tissues were collected, respectively.

A single infusion of rifapentine (30 mg/kg) was given over 15 min to a group of three healthy rabbits followed by sacrifice of one animal at each of the following time points—2, 6, and 15 hours after dosing—to establish the PK of rifapentine in rabbits. Blood was drawn from the central ear artery at the following times: before dosing at 30 min and at each 1-hour interval after dosing (up to 6 hours), as well as just before sacrifice. The lung was harvested after euthanization, and the lung tissues were collected for drug quantification using MALDI-MSI. Methods for LC-MS/MS, MALDI-MSI, and PET-CT imaging can be found in the Supplementary Materials.

Single- and multiple-dose rifampin or rifapentine treatment of Mtb-infected rabbits

Drug doses and PK sampling times for experiments in infected rabbits were selected on the basis of PK modeling of LC-MS/MS results from plasma and tissue PK studies in uninfected rabbits. Infected rabbits were ready for single- and multiple-dosing experiments once one or more cavities formed in their lungs. Rifampin (10 mg/kg) or rifapentine (30 mg/kg) was

used for single-dosing experiments, so groups of three infected rabbits were given 8 ml of rifampin (5 mg/ml) over 10 min or 12 ml rifapentine (10 mg/ml) over 15 min. Blood was drawn at 30 min and at the end of each 1-hour interval after dosing (up to 3 hours) and at the time points immediately preceding sacrifice (2, 3, and 6 hours after dosing, denoted as S2h, S3h, and S6h), for plasma PK measurement. For multiple dosing, rifampin was given at a dose of 10 mg/kg (8 ml of 5 mg/ml of rifampin solution) every 4 hours for a total of four doses. Rifapentine was given at a dose of 20 mg/kg (8 ml of 10 mg/ml of rifapentine solution) every 3 hours for a total of four doses. After the final dose of each drug, rabbits were sacrificed either 2 hours (denoted as M2h) or 12 hours after dosing (M12h) (two animals per sacrifice time per drug). Blood was collected for plasma PK measurement at 30 min after each dose and at the end of each interval, as well as at the time point just before sacrifice. After anesthesia and euthanasia, lungs were harvested to separate uninvolved lung tissues, cellular lesions, tissues surrounding the lesion (1-mm around lesion), necrotic lesions, and cavity lesions by gross pathology. For analytical drug measurement, lesions were carefully dissected away from the surrounding tissue. A cavitary lesion was further separated into fibrous cavity wall and caseous contents or interior caseum. The portions of the lesions for MALDI-MSI, H&E staining, and acid-fast staining were left embedded in the surrounding tissues to allow for examination of the spatial distribution of drugs and for confirmation of gross pathology. Sample collection and processing for MALDI-MSI and LC-MS/MS are shown in the Supplementary Materials. Tissue replicates (three to six) were collected from each compartment from the diseased rabbit during surgical operations.

PK modeling

A nonlinear mixed-effects analysis was performed by simultaneously modeling all available plasma and tissue drug concentration data for rifampin and rifapentine. With this population approach, the central tendency in the population (that is, the typical value), as well as the variability (for example, between subject variability and residual error), were quantified. This approach allowed for utilization of all available data. The model-building process was performed in a stepwise fashion, developing first the structural plasma PK model, including variability. In the second step, a full model also describing penetration into the lung and different lesion types was developed, keeping the parameters of the plasma PK model fixed (fig. S5). As a last step, all model parameters were estimated using all available data. Goodness of fit plots computed in the Xpose (version 4.0) program was also used to guide model selection. A translational model was then developed in which site-of-action PK derived from the animal model was substituted into a PK/PD model comprising clinical data from two phase 2 clinical trials. Detailed information describing the model-building process is shown in the Supplementary Materials and includes the rabbit plasma PK model, rabbit tissue penetration models, and the translational model that includes data from the clinical trials.

Statistical analysis

For the PK drug studies, means and SDs were calculated for drug concentrations in plasma and lung tissues. Differences between calculated means were compared using a two-tailed Student's *t* test. $P \leq 0.05$ was considered statistically significant. For PK drug modeling, the likelihood ratio test was used to evaluate statistical significance for inclusion of additional

parameters in nested models, assuming that the objective function value (OFV) is χ^2 distributed; thus, a decrease in OFV of 3.84 points between hierarchical models with one parameter differing was considered to be a statistical difference with a 5% significance level. For the ^{11}C-rifampin PET-CT imaging data, *P* values for comparisons of drug distribution between two compartments were calculated using a two-tailed Wilcoxon-matched pairs signed-rank test (GraphPad).

Supplementary Material

Refer to Web version on PubMed Central for supplementary material.

Acknowledgments

We thank Sanofi for supplying the study drugs rifampin and rifapentine, the Tuberculosis Trials Consortium for their generosity in sharing clinical data for translational models, the Clinical Pharmacology Analytical Laboratory at Johns Hopkins University for development and validation of the tissue assays, and T. Hoang for assistance with drug formulation.

Funding: This project was funded by an AIDS Clinical Trials group (ACTG) Novel Formulations Project Award (subaward from Brigham and Women's Hospital, NIH UM1AI068636-09). Other support included NIH R01-EB020539 (S.K.J.) and NIH Shared Instrument Grant S10OD018072.

REFERENCES AND NOTES

1. WHO. Global Tuberculosis Report. World Health Organization; 2017. www.who.int/tb/publications/global_report/gtbr2017_main_text.pdf
2. Prideaux B, Via LE, Zimmerman MD, Eum S, Sarathy J, O'Brien P, Chen C, Kaya F, Weiner DM, Chen P-Y, Song T, Lee M, Shim TS, Cho JS, Kim W, Cho SN, Olivier KN, Barry CE III, Dartois V. The association between sterilizing activity and drug distribution into tuberculosis lesions. Nat Med. 2015; 21:1223–1227. [PubMed: 26343800]
3. Campbell EA, Korzheva N, Mustaev A, Murakami K, Nair S, Goldfarb A, Darst SA. Structural mechanism for rifampicin inhibition of bacterial rna polymerase. Cell. 2001; 104:901–912. [PubMed: 11290327]
4. Dorman SE, Savic RM, Goldberg S, Stout JE, Schluger N, Muzanyi G, Johnson JL, Nahid P, Hecker EJ, Heilig CM, Bozeman L, Feng P-J, Moro RN, MacKenzie W, Dooley KE, Nuermberger EL, Vernon A, Weiner M. Tuberculocis Trials Consortium. Daily rifapentine for treatment of pulmonary tuberculosis A randomized, dose-ranging trial. Am J Respir Crit Care Med. 2015; 191:333–343. [PubMed: 25489785]
5. Dorman SE, Goldberg S, Stout JE, Muzanyi G, Johnson JL, Weiner M, Bozeman L, Heilig CM, Feng P-J, Moro R, Narita M, Nahid P, Ray S, Bates E, Haile B, Nuermberger EL, Vernon A, Schluger NW. Substitution of rifapentine for rifampin during intensive phase treatment of pulmonary tuberculosis: Study 29 of the tuberculosis trials consortium. J Infect Dis. 2012; 206:1030–1040. [PubMed: 22850121]
6. Dooley KE, Bliven-Sizemore EE, Weiner M, Lu Y, Nuermberger EL, Hubbard WC, Fuchs EJ, Melia MT, Burman WJ, Dorman SE. Safety and pharmacokinetics of escalating daily doses of the antituberculosis drug rifapentine in healthy volunteers. Clin Pharmacol Ther. 2012; 91:881–888. [PubMed: 22472995]
7. Rosenthal IM, Zhang M, Williams KN, Peloquin CA, Tyagi S, Vernon AA, Bishai WR, Chaisson RE, Grosset JH, Nuermberger EL. Daily dosing of rifapentine cures tuberculosis in three months or less in the murine model. PLOS Med. 2007; 4:e344. [PubMed: 18092886]
8. Savic RM, Weiner M, MacKenzie WR, Engle M, Whitworth WC, Johnson JL, Nsubuga P, Nahid P, Nguyen NV, Peloquin CA, Dooley KE, Dorman SE. Tuberculosis Trials Consortium of the Centers for Disease Control and Prevention. Defining the optimal dose of rifapentine for pulmonary

tuberculosis: Exposure-response relations from two phase II clinical trials. Clin Pharmacol Ther. 2017; 102:321–331. [PubMed: 28124478]

9. Sakamoto K. The pathology of *Mycobacterium tuberculosis* infection. Vet Pathol. 2012; 49:423–439. [PubMed: 22262351]
10. Dannenberg AM Jr, Sugimoto M. Liquefaction of caseous foci in tuberculosis. Am Rev Respir Dis. 1976; 113:257–259. [PubMed: 816235]
11. Kjellsson MC, Via LE, Goh A, Weiner D, Low KM, Kern S, Pillai G, Barry CE III, Dartois V. Pharmacokinetic evaluation of the penetration of antituberculosis agents in rabbit pulmonary lesions. Antimicrob Agents Chemother. 2012; 56:446–457. [PubMed: 21986820]
12. Boman G, Ringberger VA. Binding of rifampicin by human plasma proteins. Eur J Clin Pharmacol. 1974; 7:369–373. [PubMed: 4138537]
13. Dannenberg, AM, Jr. Pathogenesis of Human Pulmonary Tuberculosis. ASM Press; 2006. Stages in the pathogenesis of human and rabbit tuberculosis; p. 22-33.
14. Dickinson JM, Mitchison DA. Experimental models to explain the high sterilizing activity of rifampin in the chemotherapy of tuberculosis. Am Rev Respir Dis. 1981; 123:367–371. [PubMed: 6784622]
15. Gumbo T, Lenaerts AJ, Hanna D, Romero K, Nuermberger E. Nonclinical models for antituberculosis drug development: A landscape analysis. J Infect Dis. 2015; 211(Suppl 3):S83–S95. [PubMed: 26009617]
16. Ordonez AA, Tasneen R, Pokkali S, Xu Z, Converse PJ, Klunk MH, Mollura DJ, Nuermberger EL, Jain SK. Mouse model of pulmonary cavitary tuberculosis and expression of matrix metalloproteinase-9. Dis Model Mech. 2016; 9:779–788. [PubMed: 27482816]
17. Harper J, Skerry C, Davis SL, Tasneen R, Weir M, Kramnik I, Bishai WR, Pomper MG, Nuermberger EL, Jain SK. Mouse model of necrotic tuberculosis granulomas develops hypoxic lesions. J Infect Dis. 2012; 205:595–602. [PubMed: 22198962]
18. Zhang M, Li S-Y, Rosenthal IM, Almeida DV, Ahmad Z, Converse PJ, Peloquin CA, Nuermberger EL, Grosset JH. Treatment of tuberculosis with rifamycin-containing regimens in immune-deficient mice. Am J Respir Crit Care Med. 2011; 183:1254–1261. [PubMed: 21330452]
19. Jindani A, Harrison TS, Nunn AJ, Phillips PPJ, Churchyard GJ, Charalambous S, Hatherill M, Geldenhuys H, McIlleron HM, Zvada SP, Mungofa S, Shah NA, Zizhou S, Magweta L, Shepherd J, Nyirenda S, van Dijk JH, Clouting HE, Coleman D, Bateson ALE, McHugh TD, Butcher PD, Mitchison DA. RIFAQUIN Trial Team. High-dose rifapentine with moxifloxacin for pulmonary tuberculosis. N Engl J Med. 2014; 371:1599–1608. [PubMed: 25337749]
20. Gillespie SH, Crook AM, McHugh TD, Mendel CM, Meredith SK, Murray SR, Pappas F, Phillips PPJ, Nunn AJ. Four-month moxifloxacin-based regimens for drug-sensitive tuberculosis. N Engl J Med. 2014; 371:1577–1587. [PubMed: 25196020]
21. Merle CS, Fielding K, Sow OB, Gninafon M, Lo MB, Mthiyane T, Odhiambo J, Amukoye E, Bah B, Kassa F, N'Diaye A, Rustomjee R, de Jong BC, Horton J, Perronne C, Sismanidis C, Lapujade O, Olliaro PL, Lienhardt C. A four-month gatifloxacin-containing regimen for treating tuberculosis. N Engl J Med. 2014; 371:1588–1598. [PubMed: 25337748]
22. Sarathy JP, Zuccotto F, Hsinpin H, Sandberg L, Via LE, Marriner GA, Masquelin T, Wyatt P, Ray P, Dartois V. Prediction of drug penetration in tuberculosis lesions. ACS Infect Dis. 2016; 2:552–563. [PubMed: 27626295]
23. Kim M-J, Wainwright HC, Locketz M, Bekker L-G, Walther GB, Dittrich C, Visser A, Wang W, Hsu F-F, Wiehart U, Tsenova L, Kaplan G, Russell DG. Caseation of human tuberculosis granulomas correlates with elevated host lipid metabolism. EMBO Mol Med. 2010; 2:258–274. [PubMed: 20597103]
24. Luna B, Kubler A, Larsson C, Foster B, Bagci U, Mollura DJ, Jain SK, Bishai WR. In vivo prediction of tuberculosis-associated cavity formation in rabbits. J Infect Dis. 2015; 211:481–485. [PubMed: 25117755]
25. Kubler A, Larsson C, Luna B, Andrade BB, Amaral EP, Urbanowski M, Orandle M, Bock K, Ammerman NC, Cheung LS, Winglee K, Halushka M, Park JK, Sher A, Friedland JS, Elkington PT, Bishai WR. Cathepsin K contributes to cavitation and collagen turnover in pulmonary tuberculosis. J Infect Dis. 2016; 213:618–627. [PubMed: 26416658]

26. Subbian S, Tsenova L, O'Brien P, Yang G, Kushner NL, Parsons S, Peixoto B, Fallows D, Kaplan G. Spontaneous latency in a rabbit model of pulmonary tuberculosis. Am J Pathol. 2012; 181:1711–1724. [PubMed: 22960076]

27. Dooley KE, Savic RM, Park J-G, Cramer Y, Hafner R, Hogg E, Janik J, Marzinke MA, Patterson K, Benson CA, Hovind L, Dorman SE, Haas DW. ACTG A5311 Study Team. Novel dosing strategies increase exposures of the potent antituberculosis drug rifapentine but are poorly tolerated in healthy volunteers. Antimicrob Agents Chemother. 2015; 59:3399–3405. [PubMed: 25824215]

28. Nedeltchev GG, Raghunand TR, Jassal MS, Lun S, Cheng QJ, Bishai WR. Extrapulmonary dissemination of *Mycobacterium bovis* but not *Mycobacterium tuberculosis* in a bronchoscopic rabbit model of cavitary tuberculosis. Infect Immun. 2009; 77:598–603. [PubMed: 19064634]

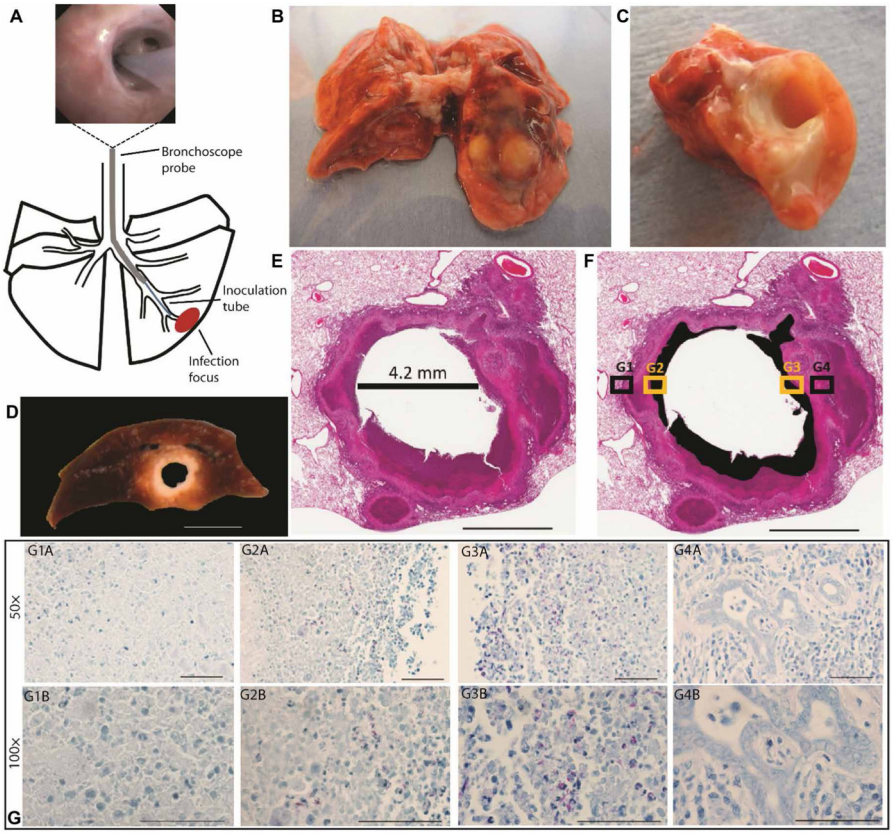

Fig. 1. Disease lesions in the rabbit model of pulmonary cavitary TB

(**A**) Diagram showing the method of bronchoscopic Mtb infection of the rabbit lung. Thick black lines show outline of lung lobes, thin black lines show the outline of bronchi, the gray line shows the bronchoscope probe, the blue line shows the inoculation tube, and the red oval shows the infection focus. Top image shows placement of the bronchoscope past the tertiary bronchial division. (**B**) Freshly resected rabbit lung showing gross pathology at the focus of Mtb infection. (**C**) Transverse section through the tubercolosis (TB) lesion in the rabbit lung in (B) confirming presence of a cavity. (**D**) Formalin-fixed cavity in the lower lung lobe of the rabbit model similar to the cavity in (C). (**E**) Hematoxylin and eosin (H&E) staining of a formalin-fixed representative cavity formed in rabbit lung after bronchoscopic infection with Mtb. The diameter of the cavity after fixation was 4.2 mm. (**F**) A modification of the same image in (E). The black sections identify areas of necrosis that were grossly identified as caseum (liquefied cell debris) in (D). (**G**) A fixed tissue section serial to the one in (E). The tissue section was formalin fixed and acid-fast stained; Mtb bacteria are stained red, other cells are blue. (G1A) to (G4A) show four fields of view taken at 50× corresponding to the box insets G1 to G4 in (F). (G1A) and (G4A) show regions of the cavity wall in (F) box insets G1 and G4 (black); (G2A) and (G3A) show regions of caseum/necrosis in (F) box insets G2 and G3 (yellow). (G1B) to (G4B) show four fields of view taken at 100× corresponding to the box insets G1 to G4 in (F). Scale bars, 10 mm (D), 3 mm (E and F), and 50 μm (G).

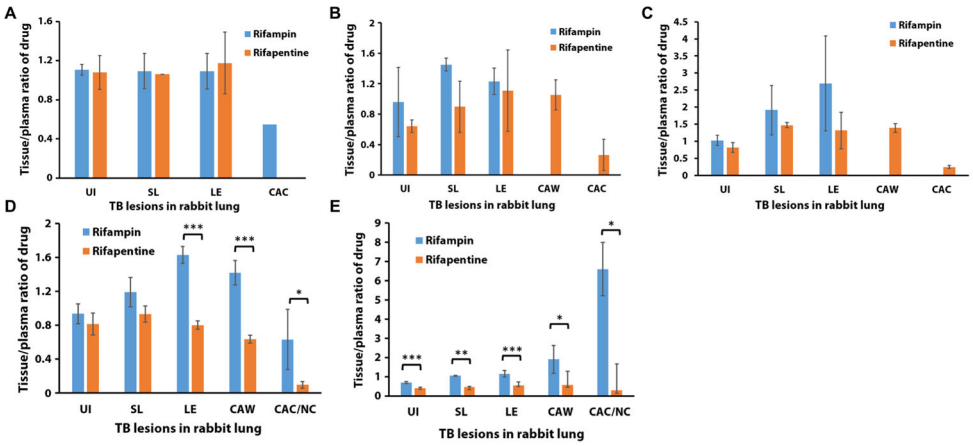

Fig. 2. Tissue-to-plasma drug concentration ratios after treatment of the rabbit TB model

Rabbits received either a single dose of rifampin or rifapentine antibiotic or the final dose of a multiple-dosing regimen. (**A**) Two hours after a single dose of rifampin or rifapentine, (**B**) 3 hours after a single dose of rifampin or rifapentine, (**C**) 6 hours after a single dose of rifampin or rifapentine, (**D**) 2 hours after the final dose of rifampin or rifapentine, and (**E**) 12 hours after the final dose of rifampin or rifapentine. For analysis of drug concentrations in lung tissue, three to six tissue replicates were collected from each compartment of the diseased rabbit lung after necropsy at different time points after intravenous injection of drug. The tissue-to-plasma ratios of drug concentration were calculated as follows: The drug concentration in tissue was divided by the drug concentration in plasma, which was collected before sacrifice of the rabbit. $*P < 0.05$, $**P < 0.01$, and $***P < 0.001$, two-tailed *t* test. UI, uninvolved lung tissue; SL, tissue surrounding lesions; LE, cellular lesion; CAW, cavity wall; CAC/NC, cavity caseum/necrotic center.

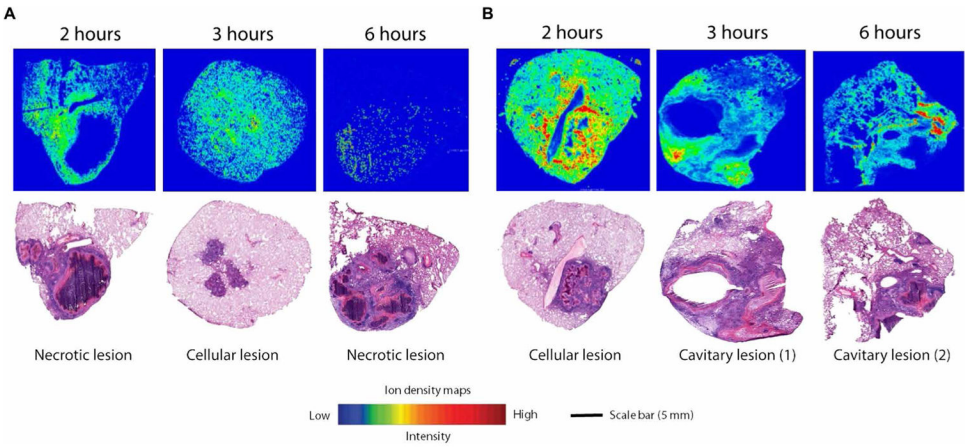

Fig. 3. MALDI-MSI analysis and gross pathology of rabbit lung after a single dose of rifampin or rifapentine

Ion density maps of rifampin (**A**) or rifapentine (**B**) in rabbit lung biopsies taken at different time points (2, 3, and 6 hours) after a single drug dose are shown. The maps show the spatial distribution of rifampin and rifapentine across the tissue sections at 2, 3, and 6 hours after dosing. Rifampin and rifapentine were observed only at low signal intensities in the caseum. All matrix-assisted laser desorption/ionization mass spectrometry (MALDI-MS) images are shown on fixed ion density scales. Images of H&E-stained lung tissue sections from the same biopsy are shown below each ion density map to confirm gross pathology and the type of lung lesion. Scale bar, 5 mm.

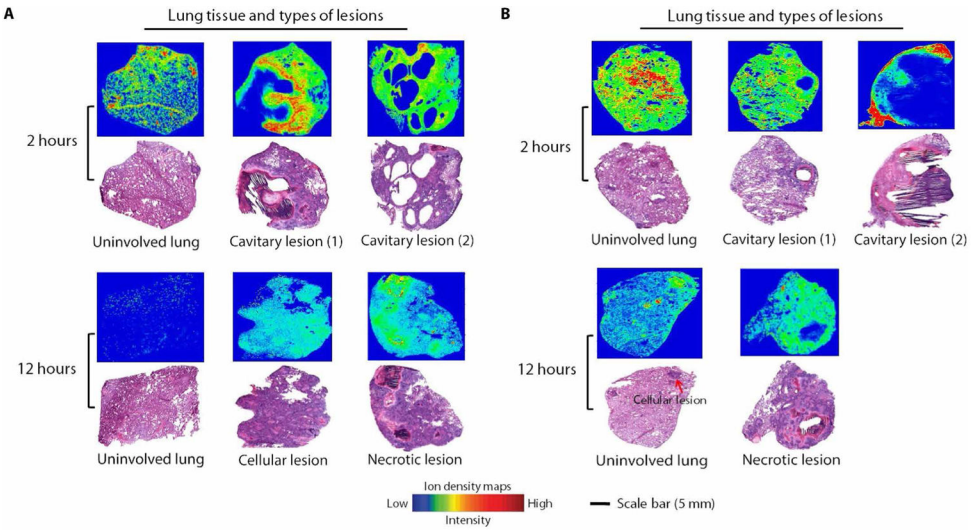

Fig. 4. MALDI-MSI analysis and gross pathology of rabbit lung after multiple doses of rifampin or rifapentine

Ion density maps of rifampin (**A**) or rifapentine (**B**) after multiple dosing in rabbit lung biopsies taken 2 or 12 hours after the final dose are shown. At 12 hours after the final dose, the rifampin signal was higher in necrotic lesions than in surrounding infected lung tissue, whereas rifapentine did not concentrate in the necrotic lesions/caseum. All MALDI-MS images are shown on a fixed ion density scale. Images of H&E-stained lung tissue sections from the same biopsy are shown below each ion density map to confirm gross pathology and the type of lung lesion. Scale bar, 5 mm.

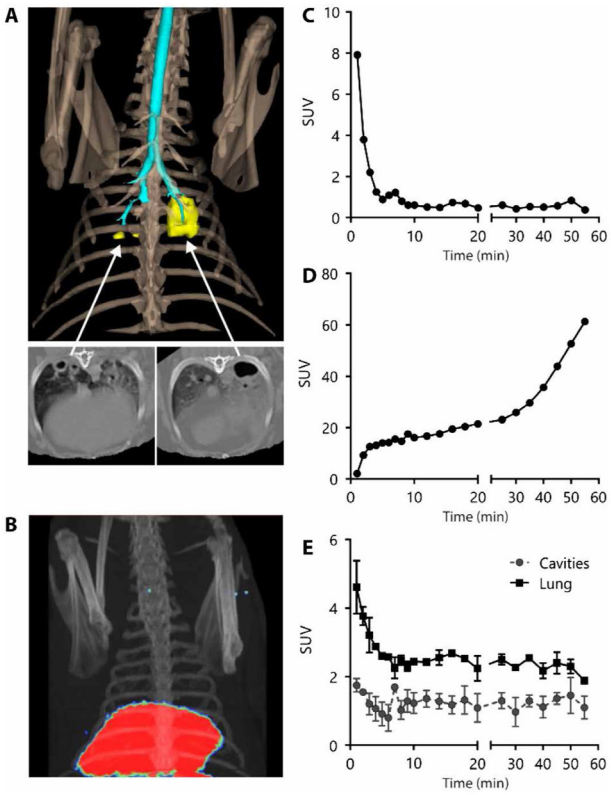

Fig. 5. ^{11}C-rifampin PET-CT imaging of an Mtb-infected rabbit with multiple cavitary lesions

(**A**) Three-dimensional CT reconstruction of the thoracic region of an Mtb-infected rabbit showing the bone (light brown), airways (cyan), and lung cavities (yellow). CT transverse views of the cavitary lesions are also shown. (**B**) Positron emission tomography (PET)–CT three-dimensional image of the same animal with the PET-CT signal localized in the liver (red) 55 min after intravenous injection of ^{11}C-rifampin. (**C**) Dynamic PET standardized uptake values (SUV) representing concentrations of ^{11}C-rifampin in rabbit blood. (**D**) Dynamic PET SUV values representing tissue concentrations of ^{11}C-rifampin in liver measured at 22 time points over a 60-min period after intravenous injection of ^{11}C-rifampin. (**E**) Mean activity of ^{11}C-rifampin represented as SUV values in three different cavitary lung lesions (each with a minimum of 200 voxels) measured at 22 time points over a 60-min period after intravenous injection of ^{11}C-rifampin. Cavity lesion tissue has a lower concentration of ^{11}C-rifampin compared to the surrounding infected lung tissue ($P < 0.0001$, two-tailed *t* test).

Table 1

Appearance of disease after bronchoscopic instillation of Mtb into rabbits

Numbers in parentheses represent time (in weeks) after infection. The terms small, some, large, and huge represent the diameter of disease lesions, ≤0.5, 0.5 to 1.0, 1.0 to 2, and ≥2 cm, respectively. *Mycobacterium tuberculosis*, *Mtb*; CFU, colony-forming factor; CT, computed tomography.

Concentration of *Mtb* H37Rv strain (CFU/ml)	Volume (in milliliters) per instillation per rabbit	First CT scan result (weeks after infection)	Second CT scan or clinical result (weeks after infection)
5×10^4	1.2	No sign of disease (3)	No disease (8)
	1.2	Small consolidation (3)	Clear (8)
	1.2	Small consolidation (3)	Clear (8)
5×10^5	0.2	Some consolidation (3)	Clear (6)
	0.4	Some consolidation (3)	Clear (6)
	0.6	Some consolidation (3)	Clear (6)
	1.2	Some consolidation (3)	Clear (8)
	1.2	Some consolidation (3)	Two cavities (6)
	1.2	Some consolidation (3)	Two cities (7)
5×10^6	0.2	Some consolidation (3)	Two cavities (6)
	0.4	Large consolidation (3)	Some diffusion (8)
	0.6	Large consolidation (3)	One cavity (3)
	1.2	Huge consolidation (3)	Sacrificed (3)
	1.2	Huge consolidation (3)	Sacrificed (3)
	1.2	Huge consolidation (3)	Sacrificed (3)
5×10^7	0.15	Large consolidation (1)	Three cavities (4)
	0.30	Large consolidation (1)	One cavity (4)
5×10^8	0.15	Large consolidation (1)	Two cavities (4)

Table 2

Rifampin and rifapentine penetration into rabbit tubercular lesions and healthy lung tissue

n, number of samples; *N*, number of animals. FIX, parameter was fixed; 1/hour, per hour; CL, clearance; V, volume of distribution; CV, coefficient of variance.

	Rifampin (sample size)	*n*/*N*	Rifapentine (sample size)	*n*/*N*
Plasma		38/8		49/11
CL (liter/hour per kg)	0.175 (3)		0.087 (26)	
V (liter/kg)	0.54 (5)		0.67 (11)	
Residual error of plasma, CV %	34 (5)		23 (15)	
IIV (CL), CV %	42 (17)		65 (30)	
IIV (V), CV %	—		30 (42)	
Correlation CL-V	—		0.59 (27)	
Uninvolved lung		15/5		42/11
Ratio of uninvolved lung/plasma	0.78 (12)		0.71 (12)	
Rate constant of plasma to uninvolved lung (1/hour)	1.29 (27)		10 FIX	
Residual variability of uninvolved lung, CV %	22 (41)		33 (38)	
Cellular lesion		20/5		19/6
Ratio of cellular lesion/plasma	1.12 (5)		1.1 (14)	
Rate constant of plasma to cellular lesion (1/hour)	0.59 (19)		1.86 (33)	
Residual variability of cellular lesion, CV %	19 (30)		27 (25)	
Tissue surrounding lesion		12/5		15/6
Ratio of tissue surrounding lesion/plasma	1.01 (16)		1.05	
Rate constant of plasma to tissue surrounding lesion (1/hour)	0.74 (138)		0.83	
Residual variability of tissue surrounding lesion, CV %	22 (55)		29	
Cavity caseum		9/3		13/4
Ratio of cavity caseum/plasma	1.11 (21)		0.25 (21)	
Rate constant of plasma to cavity caseum (1/hour)	0.086 (40)		234 (40)	
Residual variability of cavity caseum, CV %	57 (5)		60 (31)	
Cavity wall		7/2		16/4
Ratio of cavity wall/plasma	0.98 (8)		1.01 (8)	
Rate constant of plasma to cavity wall (1/hour)	0.37 (13)		0.63 (4)	
Residual variability of cavity wall, CV %	26 (42)		15 (5)	